



Published in final edited form as:

Structure. 2021 September 02; 29(9): 1029–1039.e3. doi:10.1016/j.str.2021.03.018.

Structural basis for the association of PLEKHA7 with membrane-embedded phosphatidylinositol lipids

Alexander E. Aleshin^{1,3}, Yong Yao^{1,3}, Amer Iftikhar², Andrey A. Bobkov¹, Jinghua Yu¹, Gregory Cadwell¹, Michael G. Klein¹, Chuqiao Dong², Laurie A. Bankston¹, Robert C. Liddington¹, Wonpil Im², Garth Powis¹, Francesca M. Marassi^{1,*}

¹Cancer Center, Sanford Burnham Prebys Medical Discovery Institute, 10901 North Torrey Pines Road, La Jolla CA, 92037

²Departments of Biological Sciences, Chemistry and Bioengineering, Lehigh University, PA 18015, USA

³Authors contributed equally

Summary

PLEKHA7 (pleckstrin homology domain containing family A member 7) plays key roles in intracellular signaling, cytoskeletal organization and cell adhesion, and is associated with multiple human cancers. The interactions of its pleckstrin homology (PH) domain with membrane phosphatidyl-inositol-phosphate (PIP) lipids, are critical for proper cellular localization and function, but little is known about how PLEKHA7 and other PH domains interact with membrane-embedded PIPs. Here we describe the structural basis for recognition of membrane-bound PIPs by PLEKHA7. Using X-ray crystallography, nuclear magnetic resonance (NMR), molecular dynamics (MD) simulations, and isothermal titration calorimetry (ITC), we show that the interaction of PLEKHA7 with PIPs is multivalent, distinct from a discrete one-to-one interaction, and induces PIP clustering. Our findings reveal a central role of the membrane assembly in mediating protein-PIP association and provide a roadmap for understanding how the PH domain contributes to the signaling, adhesion and nanoclustering functions of PLEKHA7.

*Address correspondence to fmarassi@sbp.edu.

Lead Contact: Francesca M. Marassi

Author contributions

Conceptualization & Supervision: F.M.M., R.C.L., W.I. and G.P.

Investigation: A.E.A., Y.Y., J.Y., A.A.B., G.C., M.G.K., L.A.B, A.I., C.D.

Writing – Original Draft: F.M.M.

Writing – Review & Editing: F.M.M., A.E.A., Y.Y. and G.P.

Visualization: F.M.M. and A.E.A.

Funding acquisition & Project Administration: F.M.M., R.C.L., W.I and G.P.

Publisher's Disclaimer: This is a PDF file of an unedited manuscript that has been accepted for publication. As a service to our customers we are providing this early version of the manuscript. The manuscript will undergo copyediting, typesetting, and review of the resulting proof before it is published in its final form. Please note that during the production process errors may be discovered which could affect the content, and all legal disclaimers that apply to the journal pertain.

Declaration of interests

GP is Director of PHusis Therapeutics. The authors declare no other potential competing interests.

Additional information

Supplementary information is available for this paper.

eTOC blurb

The interactions of PLEKHA7 with membrane-bound phosphatidylinositol (PIP) lipids are critical for cell signaling and cytoskeletal organization. Here we describe the structural basis for its PIP recognition by its PH domain and provide a roadmap for understanding how this contributes to the functions of PLEKHA7.

Keywords

PH domain; PIP; nanodisc; structure; NMR

PLEKHA7⁴ is a major component of the cytoplasmic region of epithelial adherens junctions that functions to ensure cell-cell adhesion and tight junction integrity through its interactions with cytoskeleton proteins (Meng et al., 2008; Paschoud et al., 2014; Pulimeno et al., 2010; Rouaud et al., 2020). Increased levels of human PLEKHA7 are associated with hypertension (Levy et al., 2009) and glaucoma (Awadalla et al., 2013), and PLEKHA7 protein staining has been reported in several human cancers, including advanced breast, renal and ovarian cancer (Kourtidis et al., 2015; Tille et al., 2015), with highest occurrences in colon cancer (Castellana et al., 2012). A recent study (Nair-Menon et al., 2020) showed that disruption of the apical junction localization of RNA interference machinery proteins correlates with loss of PLEKHA7 in human colon tumors and poorly differentiated colon cancer cell lines, while restoration of PLEKHA7 expression restores proper localization of RNA interference components and suppresses cancer cell growth in vitro and in vivo. Moreover, we have observed (Jeung et al., 2011) that PLEKHA7 associates with proteins of the membrane-bound KRAS (Kirsten rat sarcoma viral oncogene homolog) signaling nanocluster in colon cancer cells, and that *plekha7* gene knock down inhibits the proliferation of colon cancer cells with mutated KRAS, but not normal cells with wild-type KRAS. PLEKHA7, therefore, represents an attractive druggable target for the selective inhibition of signaling and its tumor-related functions in colorectal cancer. Despite its importance, the molecular basis for the role of PLEKHA7 in these disorders is poorly understood.

The 1271-residue PLEKHA7 is one of nine family members characterized by a 120-residue N-terminal pleckstrin homology (PH) domain (Fig. S1A). PH domains are found in more than 100 different proteins, they are known for their ability to bind phosphatidyl-inositol-phosphate (PIP) lipids within cell membranes, and their association with PIPs is essential for intracellular signaling, cytoskeletal organization and the regulation of intracellular membrane transport (DiNitto and Lambright, 2006; Lemmon, 2007). Notably, PH domains can be selectively targeted by small molecules that inhibit their signaling function (Indarte et al., 2019; Meuillet et al., 2003; Meuillet et al., 2010). In the case of PLEKHA7, the PH domain is required for establishing proper subcellular localization through its interactions with PIPs (Wythe et al., 2011), and thus, could offer a new avenue for attacking cancer by inhibiting PLEKHA7 localization.

Following the first NMR structures of pleckstrin (Yoon et al., 1994) and β -spectrin (Macias et al., 1994), the structures of many other PH domains have been reported, either in their free state or complexed with soluble inositol phosphate (IP) small molecules (Moravcevic et

al., 2012). These have provided important functional insights, but little is still known about the way in which PH domains associate with full-length PIPs incorporated in membranes, and nothing is known about the structural basis for PIP binding by PLEKHA7. Using a multidisciplinary approach that combined X-ray crystallography, NMR, all-atom MD simulations, and ITC binding measurements, we have determined the structures of the PLEKHA7 PH domain and characterized its interactions with membrane-embedded PIPs with atomic-level detail. The data reveal three PLEKHA7 binding sites for PIP, and demonstrate that confinement of PIP molecules by the membrane assembly is important for promoting the multivalent association of one PH domain with multiple PIPs leading to membrane surface localization.

Results and Discussion

Structure of the PLEKHA7 PH domain.

We obtained crystals for two states of the PH domain of PLEKHA7 – one ligand-free (PHA7_{APO}) and the other bound to sulfate from the crystallization buffer (PHA7_S) – and we determined two structures, which refined to 2.80 Å and 1.45 Å resolution, respectively (Fig. 1A, B; Fig. S1C, D; Table S1). Each structure crystallized in a different space group and has two copies of the protein per crystallographic asymmetric unit, but the protein-protein interfaces differ in each case, and do not appear to reflect biologically functional dimers. PLEKHA7 adopts the PH domain signature fold (Lemmon, 2007; Lietzke et al., 2000): a seven-stranded β-barrel, capped at one end by a 16-residue α-helix. The barrel opening is highly positively charged and lined by the β1-β2, β3-β4 and β6-β7 loops which are hypervariable in both length and sequence across the PH domain family. The K173-K183-R185 motif, at the end of β1 and start of β2, forms the canonical IP binding site of PH domains (Moravcevic et al., 2012). In the case of PHA7_S, this site – denoted here as site I – is occupied by one of two sulfate anions resolved in the structure. No electron density was observed for either the β6-β7 loop or C-terminal residues S285-R298, which were included in the sequence of PHA7_S (residues 164-298) but deleted in PHA7_{APO} (residues 164-285). The structures show that the PH domain is confined to residues 16-285, and subsequent NMR, ITC and MD simulation studies utilized this trimmed sequence, henceforth referred to as PHA7 (Fig. S1B).

To further examine the protein conformation and dynamics in solution, we prepared ¹⁵N/¹³C labeled PHA7 for NMR experiments. The assigned NMR chemical shifts (¹HN, ¹⁵N, ¹³CA and ¹³CB) show that the protein adopts the same structure in solution as in its crystalline form, and that the long β6-β7 loop forms a random coil (Fig. 1D). The ¹H/¹⁵N nuclear Overhauser effect (NOE) data show that the β-strands, and helices (α1, α') all have similar (>0.8) NOE intensities, consistent with uniform backbone dynamics and conformational order (Fig. 1E). By contrast, the termini and loops have distinctly lower NOE intensities, and hence greater extents of dynamics and lower conformational order. High flexibility is observed for β6-β7 where the intensities approach zero, and also for β1-β2 and β3-β4, loops that are important for defining the recognition of specific PIP phosphorylation states by other PH domains (Lemmon, 2007).

PLEKHA7 shares 50-75% amino acid sequence identity with the other PLEKHA family members (Fig. S1F), but it is unique in containing a 20-residue insertion between β 6 and β 7. Long β 6- β 7 loops are found in other members of the larger PH domain superfamily. In GRP1 and ARNO (Cronin et al., 2004; Lietzke et al., 2000), the β 6- β 7 loop forms a β -hairpin that elongates the β -barrel, generating a more extensive pocket for binding IP, while in the case of ANLN, the loop does not appear to be involved in IP binding. The β 6- β 7 sequence of PHA7 differs from those of GRP1, ARNO and ANLN.

Interactions with soluble IP headgroups and membrane-embedded PIPs.

To assess the affinity of PHA7 for membrane-embedded PIP lipids, we performed co-sedimentation experiments with PIP-containing liposomes. While PHA7 does not sediment with pure dipalmitoyl-phosphatidyl-choline (diC16-PC) liposomes, incubation with liposomes containing 10% molar diC16-PI(3,4,5)P₃ resulted in abundant co-sedimentation (Fig. 2A). Notwithstanding this evident high affinity for PIP-rich membranes, our attempts to co-crystallize PHA7 with either short-chain PIP lipids or soluble IP headgroups – IP(4,5)P₂, IP(3,4)P₂ or IP(3,4,5)P₃ – resulted in the apo form of the protein, without bound ligand, regardless of crystallization or soaking conditions. This is in line with the μ M-range dissociation constants (K_d) that we measured by ITC for the interaction of PHA7 with soluble IPs (Fig. 2B; Table 1). The combined data indicate that PHA7 has modest affinity for soluble IPs but appreciably higher affinity for PIP lipids incorporated in membranes. A similar effect has been reported for the PH domain of kindlin 3 whose binding affinity for PIP was enhanced 1,000 fold upon PIP incorporation in nanodiscs (Ni et al., 2017).

To analyze this effect quantitatively, we performed ITC experiments with PHA7 and PIP-enriched lipid nanodiscs – nanometer-size discoidal membranes that are stabilized by two copies of a membrane scaffold protein (MSP) derived from the apolipoprotein ApoA1 (Bayburt et al., 2002). We prepared nanodiscs with either pure diC16-PC or a 1/9 molar mixture of diC16-PIP and diC16-PC. Remarkably, the ITC binding affinity measured by titrating the protein with PIP-nanodiscs is enhanced by more than one order of magnitude relative to soluble IP headgroups (Fig. 2C; Table 1), in line with the co-sedimentation results. Moreover, PHA7 now appears to display some – albeit modest – selectivity ($p < 0.05$) for PI(4,5)P₂ > PI(3,4,5)P₃ > PI(3,4)P₂ lipid membranes.

The simplified nanodisc platform, while powerful, prohibits analysis of binding stoichiometry, because the potential for lipid clustering (Wen et al., 2018) during the nanodisc preparation process makes it challenging to control the composition of individual nanodiscs. Nevertheless, the enhanced affinity for membrane-incorporated PIPs suggests that additional factors – beyond a pure one-to-one PHA7 to IP headgroup interaction – play a role in recruiting the protein to the membrane surface. The binding free energies derived from ITC offer some insights in this regard (Fig. 2D). The association of PHA7 with free IPs is highly entropy driven, with binding thermodynamics characterized by very small values of favorable enthalpy (ΔH) and a much greater entropic component (ΔS). The situation is reversed for the association of PHA7 with membrane-embedded PIPs, where the enthalpic component dominates.

We propose that this effect reflects the interaction of one PHA7 molecule with multiple PIP molecules incorporated in the nanodisc membrane, and a reduction of PHA7 and PIP conformational, rotational and translational degrees of freedom imposed by the membrane scaffold. According to the principles of binding free energy additivity (Jencks, 1981), the observed binding free energy is the sum of the intrinsic binding free energies of the individual ligands plus a “connection” energy – a largely entropic term that reflects the change in the probability of binding due to the change in translational and rotational degrees of freedom that result from connecting the ligands. Such superadditivity is well known in drug development, where chemical linking of weakly-binding fragments results in molecules with binding free energy greater than the sum of the individual fragments. In the case of the PHA7-PIP membrane complex, membrane confinement replaces chemical linking and the additional Jencks “connection” free energy may be attributed to a change in the probability of binding that results from confinement of multiple PIPs and bound PHA7 by the membrane, resulting in overall enhanced affinity. Additional factors such as interactions of the protein with the hydrophobic acyl chains of the lipids may further contribute to the enhanced affinity.

Structural basis for binding soluble IPs.

In the absence of co-crystals, the structure of PHA7_S provides useful insights about the protein’s interactions with the IP moiety. In PHA7_S (Fig. 1B; Fig. S2A) one sulfate anion occupies site I, where it is coordinated by the side chains of K173 in β 1, R185 in β 2 and Y196 at the end of β 3. A second sulfate anion binds on the opposite side of the β 1- β 2 loop – denoted here as site II – where it is coordinated by the side chains of Q174 and W182, which define the start and the end of the β 1- β 2 loop, and S226 in the middle of the β 5- β 6 loop. While IP binding at this second site is considered “atypical”, and thought to occur only in PH domains that lack the canonical binding site (Moravcevic et al., 2012), it has been observed experimentally for the PH domains of spectrin (Hyvonen et al., 1995), Tiam1 and ArhGAP9 (Ceccarelli et al., 2007), and ASAP1 (Jian et al., 2015), where both canonical and atypical sites are simultaneously bound to short-chain PI(4,5)P₂.

Notably, while the structures of PHA7_{APO} and PHA7_S are superimposable, with root mean square deviation (rmsd) of 0.49/0.52 Å (chains A-A/B-B) for CA atoms in the barrel core, they differ appreciably in the β 1- β 2 loop where the rmsd jumps to 2.54/2.42 Å (chains A-A/B-B) (Fig. S2B). In the apo structure, the β 1- β 2 loop folds towards the barrel opening and adopts a β -turn conformation that is restrained by a network of hydrogen bonds involving the K173 and K183 amino groups, the S177 hydroxyl, and the D175 carboxylate oxygens (Fig. 1A; Fig. S2C, D). The D175 side chain points into binding site I, at the center of a clasp-like structure formed by the K173 and K183 side chains. The temperature factors of the β 1- β 2 loop are twice greater than for the rest of the protein, and the loop has a distinct conformation in each of the two molecules of the crystal structure, reflecting its flexibility (Fig. S1C). In the sulfate-bound structure, on the other hand, the β 1- β 2 loop folds away from the barrel opening (Fig. 1B; Fig. S2C, D). The D175 side chain is disengaged from the K173-K183 clasp: It points into the loop, forming hydrogen bonds with its main chain atoms, and away from the sulfate anion bound in site I. The β 1- β 2 temperature factors, while higher than those of the barrel proper, are lower than those observed in PHA7_{APO}, and the

loop has the same conformation in both molecules of the structure (Fig. S1D), indicating that the bound sulfate stabilizes the β 1- β 2 loop conformation.

The structures point to D175 and the β 1- β 2 loop as important mediators of the interaction of PHA7 with IP headgroups. A previous study (Carpten et al., 2007) identified a “sentry” Glu residue in the PH domain of AKT positioned to disfavor binding of a phosphate group at the 3-position of the inositol ring and define a preference for IP(4,5)P₂ over IP(3,4)P₂ and IP(3,4,5)P₃. Changing this sentry Glu to Lys, an AKT mutation that occurs in many tumors, reverses the preference and increases the affinity for IPs by ~10-fold.

To examine the role of D175 in PHA7, we generated the D175K mutant and characterized its structure and IP binding properties. ITC measurement show that PHA7-D175K has a three-fold greater affinity for IP(4,5)P₂ ($K_d=10.7 \mu\text{M}$) and nine-fold greater affinity for IP(3,4,5)P₃ ($K_d=3.5 \mu\text{M}$) compared to wild-type (Table 1). Notably, PHA7-D175K co-crystallized with soluble IP(3,4,5)P₃. The structure refined to a resolution of 2.43 Å (Fig. 1C, Table S1) with two copies of the protein per crystallographic asymmetric unit. Once again, no electron density was observed for the long β 6- β 7 loop, indicating that it remains mobile and disordered, without apparently contributing to IP binding.

The two molecules of PHA7-D175K within the crystallographic asymmetric unit coordinate two IP(3,4,5)P₃ moieties sandwiched between them: One at the site I, and the second associated more peripherally with yet another electropositive patch – denoted here as site III – formed by the side chains of K183, R185, K198, and R201 that protrude from β 2 and from the β 3- β 4 loop (Fig. S3A). The structure reflects at least four distinct modes of IP binding by PHA7. In molecule A of the asymmetric unit the phosphate group at the fifth position of the inositol ring occupies the same position as the sulfate anion in the structure of wild-type PHA7_S, while in molecule B the binding geometry is flipped such that it is the phosphate group in first position that coincides with the sulfate binding site (Fig. S3B, C). Binding of the peripheral IP(3,4,5)P₃ at site III is similarly mirrored in each copy of PHA7-D175K, resulting in two possible binding geometries. Moreover, the involvement of K183 and R185 in both sites I and III reflects plasticity in the PHA7-IP interaction.

To further examine the interaction of wild-type PHA7 with IPs, we performed NMR experiments in solution. Addition of soluble IP(3,4,5)P₃ into ¹⁵N-labeled PHA7 resulted in specific ¹H/¹⁵N chemical shift perturbations that map to the PHA7 barrel opening (Fig. 3A-C). In line with the ITC data, NMR reflects a weak binding interaction with fast exchange binding dynamics (Williamson, 2013). No major structural reorganization of either the core or the β 6- β 7 loop of PHA7 is observed, but signals from all three binding sites identified by crystallography are perturbed (Fig. 3D, E), with the largest changes observed for the β 1- β 2 and β 3- β 4 loops and residues at the start of β 7, including key residues (Q174, D175, S177, K183, R185, Y260) identified in the structures of PHA7_S and PHA7-D175K. We conclude that the interaction of PHA7 with soluble IP headgroups is structurally plastic, with three potential binding sites for inositol phosphate localized across the electropositive barrel opening, and low selectivity for a specific orientation of the IP(3,4,5)P₃ moiety.

Structural basis for binding membrane PIPs.

The structural and ITC binding data show that PHA7 has modest affinity for freely soluble IP ligands but appreciably higher affinity for PIP-rich lipid bilayers, pointing to the importance of the PIP membrane environment. To explore the interaction with PIP membranes at the atomic level, we performed NMR experiments with ^{15}N labeled PHA7 and PIP-nanodiscs. Incubation of PHA7 with diC16-PC nanodiscs, resulted in no detectable NMR spectral changes (Fig. 4A; S4A). This is consistent with the liposome co-sedimentation results and confirms the inability of PHA7 to bind membranes devoid of PIP. Incubation with nanodiscs containing 10% molar diC16-PI(3,4,5) P_3 gave a dramatically different result: The NMR spectrum was effectively obliterated, except for peaks from sites in the termini and the flexible $\beta 6$ - $\beta 7$ loop (Fig. 4B; S4B). We interpret such massive peak suppression to reflect immobilization of the relatively small, 125-residue protein, caused by its association with the comparatively large nanodisc membrane. Moreover, since both PC and PIP nanodisc preparations have similar and homogeneous size distributions (~ 8 nm radius; Fig. S4D), we attribute the peak suppression effect to a PIP-dependent association of the protein with the nanodisc membrane that is long-lived on the msec time scale of $^1\text{H}/^{15}\text{N}$ correlation NMR experiment.

Increasing the temperature restored the NMR spectrum (Fig. 4C; Fig. S4C), and while this is expected to enhance the binding exchange dynamics, it also allowed us to map specific chemical shift perturbations that reflect the interaction of PHA7 with the PIP nanodisc membrane. The perturbations (Fig. 4D) mirror the profile observed with free IP(3,4,5) P_3 (Fig. 3D), but map to more extended regions of $\beta 1$ and $\beta 2$, and include sites in $\beta 5$ - $\beta 6$. The largest perturbations map to the $\beta 1$ - $\beta 2$ hairpin, the $\beta 3$ - $\beta 4$ loop, and the start of $\beta 7$, implicating binding sites I, II and III in PIP-mediated membrane association, and indicating that PHA7 uses all three to dock onto the PIP-membrane surface.

All atom MD simulations provide molecular context for the NMR data. We performed ten independent, unrestrained, 1- μs MD simulations of PHA7 for each of three different lipid bilayer membranes similar to the experimental nanodiscs (Table S2). All ten simulations with either PI(4,5) P_2 or PI(3,4,5) P_3 resulted in rapid membrane surface association of PHA7, which remained membrane-bound throughout the course of 1- μs simulation, while little evidence of binding to PC-only membranes was observed (Fig. S5A-C). In all cases, PHA7 adopts a preferred orientation at the PIP membrane surface, with the $\beta 3$ strand at an average angle of 35° from the membrane normal, the C-terminal helix exposed to bulk water, and sites I, II and III docked on the membrane (Fig. 4E; Fig. S5D, E).

Notably, the interaction patterns from unrestrained MD simulations mirror the experimental NMR perturbation profile (Fig. 5A, B). Protein sites with NMR signals that are sensitive to PIP-nanodiscs also interact with the PIP membrane surface in the MD simulations. Viewed in a snapshot of MD simulation with a PI(3,4,5) P_3 membrane (Fig. 4E), the NMR perturbations are associated with membrane-binding sites. These include conserved hydrophobic residues (L181, M179) in the $\beta 1$ - $\beta 2$ loop that insert deeply into the hydrophobic core of the membrane, thereby providing added stability to the interaction. The PH domain orientation at the membrane surface is remarkably similar to that observed from EPR-guided MD simulations of GPR1 with PIP membranes (Lai et al., 2013). In that

study, hydrophobic interactions between GPR1 side chains and the membrane core were also observed, indicating that superficial membrane penetration helps stabilize a specific geometry of PH domain association with the membrane surface.

In line with this observation, the time-averaged root mean-squared fluctuations (RMSF), calculated for heavy atoms over the last 500 ns of 1- μ s MD trajectories, show that the β 1- β 2 loop experiences a marked reduction in conformational flexibility upon binding PIP membranes (Fig. 5C). By contrast this effect is not observed for PC membranes. Moreover, while the long β 6- β 7 loop remains highly flexible in both the soluble and membrane-associated states of PHA7, the length of its flexible region is significantly reduced. At the molecular level, the loop fluctuations are dampened at its edges, where R239 and R258 engage with a PIP phosphate group and E253 helps stabilize the interaction.

Closer examination of the PHA7-PIP membrane assembly reveals multivalent interactions of the protein with PIPs. A total of seven PI(3,4,5)P₃ molecules establish close contacts ($> 4\text{\AA}$) with the protein: Two PIP molecules associate with each of sites I and III, and three associate in the periphery of site II (Fig. 5D; Fig. S5F). In this way, PHA7 recruits a cluster of PIP molecules to its periphery. The data demonstrate that PHA7 established multivalent interactions with membrane PIPs. These are primarily electrostatic, involving basic sidechains and inositol ring phosphate groups, but also include hydrogen bonds from polar side chains, and hydrophobic contacts between nonpolar side chains and the lipid acyl chains. These results help explain the enhanced affinity of PHA7 for PIP membranes compared to freely soluble IPs.

Finally, we performed NMR experiments with short-chain diC8-PIP phospholipids into ¹⁵N-labeled PHA7. The chemical shift perturbations (Fig. 6) mirror those observed with soluble IP (Fig. 3) and PIP nanodiscs (Fig. 4), but also display notable differences: diC8-PIPs perturb additional hydrophobic sites (e.g. L188, C192, L193, I208, V273) deep inside the β -barrel of the PH domain to helix α 1, indicating that the acyl chains associate with hydrophobic patches in the barrel interior. Interestingly, association of the acyl chains with the β -barrel interior appears to be predicated upon binding of the PIP headgroup with PHA7, since the addition of non-phosphorylated diC8-PI induced no perturbations in the NMR spectrum of PHA7 (Fig. 6A).

Caution must be exercised in interpreting the effects of micellar detergents like diC8-PIPs, and we note that acyl chain penetration of the PH domain β -barrel is not observed for PIP lipids embedded in the nanodisc membrane. Nonetheless, such interactions are not unprecedented, and may reflect an alternate function of the PH domain. For example, the serum retinol binding protein (Cowan et al., 1990) and fatty acid binding protein (Sacchettini et al., 1989) adopt a β -barrel structure that is very similar to that of PH domains, and each bind a retinol or acyl chain deep into their β -barrel. Moreover, MD simulations of Grp1 with PIP membranes (Lumb et al., 2011) indicate that the Grp1 PH domain associates with membrane PIPs sufficiently tightly to pluck a single PIP phospholipid from the bilayer membrane assembly. In light of these studies, the finding that PIP lipid acyl chains associate with the PLEKHA7 PH β -barrel is intriguing, and suggestive of a functional role for the

PH domain of PLEKHA7 that extends beyond membrane association, and may include lipid shuttling and regulation of PIP lipid mobility in the cell.

Conclusions

PLEKHA7 relies on the interactions of its PH domain with PIPs for proper localization to the plasma membrane surface and for its normal functions (Wythe et al., 2011). Using a multidisciplinary approach, we have defined the major elements of PIP recognition by the PLEKHA7 PH domain and demonstrated the important role of the membrane scaffold in mediating its interaction with PIPs.

Although PH domains share a common fold and sequence homology, their PIP affinities and selectivities vary broadly. ITC shows that PLEKHA7 has modest affinity for free IP headgroups and no detectable selectivity for phosphorylation at specific inositol ring sites. By contrast, the binding affinity for PIP membranes is highly enhanced. Compared to freely soluble IP headgroups, the interaction with membrane PIPs is enthalpy-driven and exhibits slight selectivity for PI(4,5)P₂ (> PI(3,4,5)P₃ > PI(3,4)P₂) relative to the other phosphorylation types. PI(4,5)P₂ is the major PIP lipid present in the inner leaflet of the plasma membrane of mammalian cells. Its phosphorylation by PI 3-kinase (PI3K) produces PI(3,4,5)P₃, a key second messenger in pathways related to cell survival and metabolism, while dephosphorylation of PI(3,4,5)P₃ by phosphatases produces PI(3,4)P₂ (Cantley, 2002). Low PIP selectivity is in line with the observations (Wythe et al., 2011) that PLEKHA7 membrane targeting is not linked to the PI3 kinase-dependent conversion of PI(4,5)P₂ to PI(3,4,5)P₃ in cells, and that its PH domain is promiscuous for PI(4)P₁, PI(4,5)P₂, PI(3,4,5)P₃, as well as other non-inositol phospholipids with accessible phosphate groups, in lipid overlay assays.

Notwithstanding the relatively low selectivity of PLEKHA7 for specific inositol phosphates, the NMR data show that it does not bind short-chain diC8-PI. We conclude therefore, that phosphorylated inositol is required for binding PLEKHA7 and recruiting it to the membrane. While surface electrostatics from non-PIP acidic lipids, such as phosphatidylserine, has been shown to play a role in membrane recruitment of some PH domains (Lai et al., 2013), the data for PLEKHA7 indicate an affinity for phosphorylated inositol.

The crystal structures reveal three positively charged binding sites for the phosphate groups of the PIP headgroup moiety, and the NMR data show that all three sites engage with soluble IP headgroups, forming an extended binding surface at the open end of PH domain β -barrel. Notably, NMR studies with PIP nanodiscs show that the same binding sites, plus conserved hydrophobic residues in the β 1- β 2 loop, engage with membrane-embedded PIPs leading to membrane surface association of the PH domain that is long-lived on the msec time scale. Moreover, the MD simulations show that PLEKHA7 interacts with the PIP membrane in two ways: by engaging the phosphate groups of multiple PIP molecules through electrostatic interactions with its three binding sites, and by inserting hydrophobic side chains into the hydrophobic core of the lipid bilayer membrane. This multivalent binding interaction results in long-lived association of PH domain with the PIP membrane, on the μ s time scale of the MD simulations.

The results further indicate that PLEKHA7 induces membrane PIP clustering. We note that our simplified nanodiscs and membrane systems have both restricted geometries and PIP concentrations that are ten times higher than cells – conditions that are likely to favor cluster formation. In cells, the reverse situation, where PLEKHA7 binds to pre-formed PIP clusters, is also possible. While the cellular levels of PI(4,5)P₂ are low (~1% of total lipid), clustering is thought to increase its local concentration at specific membrane sites. A recent study (Wen et al., 2018) demonstrated that physiological levels of divalent and trivalent metal ions can induce cluster formation of very low PIP concentrations (< 0.05 mol% of total lipids). The ability to form such cation-bridged PIP clusters at extremely low concentrations reveals an important property of this central lipid, and provides evidence for the formation of distinct pools of PIP in cellular membranes, with fundamental consequences for biological function. As noted by Feigenson and colleagues (Wen et al., 2018), cation-induced PIP clustering would dampen the functions of proteins that bind free PIP lipids while enhancing the functions of proteins that bind clusters preferentially.

Clustering of PIP molecules around PH domains has also been observed in coarse-grained MD simulations, and has been proposed to contribute to the binding free energy (Yamamoto et al., 2020). Notably, two cooperative PIP-binding sites have been observed experimentally in the PH domain of ASAP1, and this has been proposed to enable rapid switching between active and inactive states during cellular signaling (Jian et al., 2015). Association with multiple PI(4,5)P₂ molecules was recently shown to both trigger an allosteric conformational switch in the ASAP1 PH domain, and maintain it in a well-defined orientation primed for functional protein-protein interactions, suggesting that PIP lipids have functionalities beyond simple membrane targeting modules (Soubias et al., 2020). Notably, PIP-mediated membrane association has also been shown to regulate KRAS functionality (Cao et al., 2019), and this has potential implications for the role of PLEKHA7 in regulating the KRAS signaling nanocluster in colon cancer cells.

For PLEKHA7, we identified three binding sites, and found that all three are engaged upon addition of either soluble IPs or PIP membranes, leading us to conclude that multivalent association is operative in both settings. Nevertheless, the membrane assembly is fundamentally important. The MD simulations indicate that PLEKHA7 establishes additional hydrophobic interactions with the membrane hydrocarbon core and adopts a preferred orientation at the membrane surface. Moreover, confinement of PIP molecules by the membrane scaffold reduces the degrees of freedom of the system to a single binding interface. We propose that these factors cooperate to lower the binding free energy and enhance the affinity of protein association with PIP membranes.

While most experimental studies have focused on the interactions of PH domains with soluble IP headgroups, our results provide atomic-level insights about the affinity of PLEKHA7 for full-length membrane-embedded PIPs. They highlight the central function of the membrane assembly and provide a roadmap for understanding how the functions of the PH domain integrate with the signaling, adhesion and nanoclustering functions of full-length PLEKHA7 in cells.

STAR Methods

RESOURCE AVAILABILITY

Lead Contact.—Further information and requests for resources and reagents should be directed to and will be fulfilled by the lead contact, Francesca M. Marassi (fmarassi@sbp.edu).

Materials Availability.—Plasmids generated in this study are available upon request.

Data and Code Availability.—The structural atomic coordinates generated in this study are available at the Protein Data Bank (PDB accession codes 7kk7, 7kjo and 7kzj). The assigned NMR chemical shifts are available at the BMRB databank (BMRB accession code 50512).

EXPERIMENTAL MODEL AND SUBJECT DETAILS

E. coli BL21 cells were used for protein expression and purification. For crystallography and ITC the bacterial cells were grown at 37°C, in LB media. For NMR studies, the bacteria were grown in M9 minimal media containing (¹⁵NH₄)₂SO₄ and/or ¹³C-glucose (Cambridge Isotope Laboratories), to obtain isotopically labeled protein.

METHOD DETAILS

Protein preparation.—The sequences (Fig. S1B) of human PLEKHA7 were cloned into the BamHI and XhoI restriction sites of the pGEX-6P-1 plasmid, and expressed in *E. coli* BL21 cells. For crystallography and ITC the bacterial cells were grown at 37°C, in LB media. For NMR studies, the bacteria were grown in M9 minimal media containing (¹⁵NH₄)₂SO₄ and/or ¹³C-glucose (Cambridge Isotope Laboratories), to obtain isotopically labeled protein. Protein expression was induced by adding 1 mM isopropyl-1-thio-β-D-galactopyranoside to the culture when the cell optical density at 600 nm (OD₆₀₀) reached 0.6. After growing the cells for an additional 15 hrs at 18°C, they were harvested by centrifugation (6,000 x g, 4°C, 15 min) and stored at –80°C overnight. Cells harvested from 2 L of culture were suspended in 35 mL of buffer A (25 mM Na/K phosphate, pH 7.4, 200 mM NaCl, 2 mM DTT, 1 mM EDTA), supplemented with protease inhibitors (cOmplete Mini EDTA-free cocktail; Roche), and lysed using a French Press.

The soluble fraction was isolated as the supernatant from centrifugation after cell lysis, and loaded on Glutathione Sepharose beads (GE Healthcare). The beads were washed with buffer B (25 mM Na/K phosphate, pH 7.4, 500 mM NaCl, 2 mM DTT, 1 mM EDTA), and then incubated overnight, at 40°C, with HRV 3C Protease (Genscript; 1.5 units per 1 mg of fusion protein) in buffer C (20 mM HEPES pH 7.4, 100 mM NaCl, 1 mM DTT, 1 mM EDTA). The cleaved protein was eluted with buffer II and further purified by cation exchange chromatography (HiTrap SP column, 5 ml, GE Healthcare) with a linear gradient of NaCl in buffer D (20 mM Tris-Cl, pH 8, 1 mM DTT, 1 mM EDTA).

Purified protein was concentrated to 10 mg/ml and stored frozen at –80°C. Prior to use, the protein was thawed, transferred to appropriate buffer by size exclusion chromatography

(Superdex 75 10/300, GE Healthcare), then concentrated by centrifugal ultrafiltration and kept at 4°C. Samples for NMR studies were transferred to NMR buffer (20 mM MES pH 6.0, 100 mM NaCl, 1 mM TCEP, 1 mM EDTA). For studies of PLEKHA7 with nanodiscs, the purified PH domain was added directly to preformed nanodiscs prepared in NMR buffer.

Nanodisc preparation.—Nanodiscs were prepared as described previously (Ding et al., 2015). Briefly, the phospholipids were dissolved in 1 mL of nanodisc buffer (20 mM Tris-Cl, pH 7.5, 100 mM NaCl, 1 mM EDTA) supplemented with Na-cholate to obtain a final 2:1 molar ratio of cholate per lipid. MSP1D1 h5 was produced in *E. coli*, as described (Hagn et al., 2013), then dissolved in 700 μ L of nanodisc buffer, and combined with the lipid solution. After incubation at room temperature for 1 hr, 2 g of Biobeads SM-2 (Biorad), prewashed in nanodisc buffer, were added, and the mixture was further incubated at room temperature, with gentle mixing, for 12 hr. The Biobeads were removed by centrifugation (1,000 x g, 4°C, 5 min) and the resulting nanodiscs were washed twice with one sample volume of nanodisc buffer. The nanodisc solution was concentrated using a 10 kD cutoff Vivaspin concentrator (Viva Products) and replaced with NMR buffer to obtain 500 μ L of 0.2 mM nanodiscs. The nanodisc concentration was estimated by measuring absorbance at 280 nm (A_{280}) of MSP1D1 h5, of which there are two copies per nanodisc. The distribution of PIP molecules among nanodiscs is assumed to be homogeneous, but this may not be the case. Nanodiscs were prepared with 100% diC16-PC, or 9/1 molar mixtures of diC16-PC with diC16-PI(3,4,5)P₃, diC16-PI(4,5)P₂, or diC16-PI(3,4)P₂. Analytical size exclusion chromatography (Superdex 75 10/300 GL column, GE Healthcare) was performed in NMR buffer to assess nanodisc size homogeneity.

ITC experiments.—ITC experiments were performed at 23°C, with all components in ITC buffer (15 mM Tris pH 7.6, 70 mM NaCl, 0.5 mM TCEP), using an iTC200 instrument (MicroCal). Titrations with soluble IP headgroups were performed with 50 μ M PHA7 in the ITC cell and 0.5 mM soluble IP molecules in the injection syringe. Titrations with PIP nanodiscs were performed with 15 μ M nanodiscs in the ITC cell and 0.5 mM PHA7 in the injection syringe. The protein concentrations were estimated by measuring A_{280} . Nanodisc concentrations reflect the A_{280} measurement of MSP1D1 h5. Integrated heat data were processed and analyzed with ORIGIN software (Microcal version 7.0552). The data were fit to a single-site binding model to extract the values of the dissociation constant for each titration.

Liposome co-sedimentation assays.—Dry lipids, either 100% diC16-PC, or a 9/1 molar mixture of diC16-PC and diC16-PI(4,5)P₂, were suspended in 2 mL of buffer (20 mM MES pH 6.0, 100 mM NaCl, 2 mM DTT, 1 mM EDTA) at a concentration of 3 mg/mL, then sonicated in a bath sonicator until the suspension became translucent, marking the formation of small unilamellar vesicles. A 200 μ L solution of vesicles was mixed with a 20 μ M solution of PLEKHA7 and incubated at room temperature for 2 h. Liposomes were then harvested by centrifugation in a BECKMAN Airfuge (A-100/30 rotor, 91,000 rpm) for 20 h. The supernatant and sediment fractions were separated and analyzed by SDS-PAGE.

Crystallization, X-ray data acquisition and structure determination.—All PHA7 crystals were obtained using the sitting drop method. For ligand-free PHA7_{APO}, protein solution (13 mg/ml in 180 mM NaCl, 20 mM Tris pH 8, 50 mM BisTris pH 6.0, 0.7 mM TCEP, 6 mM Na azide) was mixed with an equivalent volume of crystallization solution (20% PEG 3350, 20 mM MgCl₂, 20 mM NiCl₂, 100 mM HEPES pH 7) and equilibrated at room temperature. For PHA7_S, protein solution (30 mg/ml in 180 mM NaCl, 20 mM sodium phosphate pH 6.5, 5 mM DTT) was mixed with an equivalent volume of crystallization solution (25% glycerol, 2 M (NH₄)₂SO₄) and equilibrated at room temperature. Crystals were frozen without the addition of a cryoprotectant. For PHA7-D175K, 1.5 mM IP(3,4,5)P₃ and protein solution (15 mg/ml in 180 mM NaCl, 20 mM Tris pH 8, 30 mM BisTris pH 6, 0.5 mM TCEP, 6 mM Na azide) were mixed with an equivalent volume of crystallization solution (20% PEG 3350, 200 mM Na acetate) and equilibrated at room temperature. PHA7_S crystals appeared in 13 days and grew for an additional 7 days before freezing. PHA7_{APO} and PHA7-D175K crystals appeared after 1 day and grew for another 3 days before freezing. Crystals were frozen after addition of glycerol to final concentration 20% v/v.

X-ray diffraction data for PHA7_{APO} and PHA7_S were collected at the Advanced Light Source (Berkeley, CA) beamline 8.3.1, with a wavelength 1.116 Å and temperature of 100 K. The data for PHA7-D175K were collected on a Rigaku diffractometer with R-axis detector, with a wavelength of 1.54 Å and temperature of 100 K. The data were processed using the CCP4 suite (Winn et al., 2011), to resolution of 2.80 Å (PHA7_{APO}), 1.45 Å (PHA7_S) and 2.43 Å (PHA7-D175K). The structure of PHA7_S was solved first, with molecular replacement guided by the structure of PEPP1 (PDB: 1UPR; 52% identity). Phenix.AutoBuild (Adams et al., 2010) was used for initial model building, followed by several rounds of manual model inspection and correction in Coot (Emsley et al., 2010) and refinement by phenix.refine (Adams et al., 2010) and Refmac5 (Murshudov et al., 2011). The structures of PHA7_{APO} and PHA7-D175K were solved with Phaser (McCoy et al., 2007) using the structure of PHA7_S as molecular replacement model, and refined as for PHA7_S.

Molprobit (Chen et al., 2010) and the PDB validation server were used for structure validation throughout refinement. All structures had Ramachandran statistics with more than 95% of residues in favored positions and less than 1% outliers. Poisson-Boltzmann electrostatics were calculated in PyMOL 2.2 using APBS (Baker et al., 2001). Illustrations were prepared using PyMol 2.2.

NMR experiments.—NMR experiments were performed with 450 µl samples in NMR buffer, on a Bruker Avance spectrometer, equipped with a Bruker ¹H/¹⁵N/¹³C triple-resonance cryoprobe, operating at a ¹H frequency of 600 MHz. Assignments of the solution NMR resonances from N, HN, CA and CB were obtained using HNCA (Grzesiek and Bax, 1992) and HNCACB (Wittekind and Mueller, 1993) experiments. Chemical shifts were referenced to the H₂O resonance (Cavanagh et al., 1996). Secondary structure was characterized by analyzing the chemical shifts with TALOS+ (Cornilescu et al., 1999; Shen et al., 2009). The total differences (ΔHN) in amide ¹H and ¹⁵N chemical shifts due to the C-terminus or peptide binding were calculated by adding the changes in ¹H (ΔH) and ¹⁵N (ΔN) chemical shifts using the equation $\Delta HN = (1/2) [(\Delta H)^2 + (\Delta N)^2]$. The NMR data

were processed and analyzed using NMRPipe (Delaglio et al., 1995), Sparky (Goddard and Kneller, 2004) and NMRView (Johnson and Blevins, 1994). The NMR pulse sequences are described in detail in the literature (Bax and Grzesiek, 1993; Cavanagh et al., 1996; Clore and Gronenborn, 1998; Ferentz and Wagner, 2000; Fesik and Zuiderweg, 1990; Kay, 2001).

Molecular dynamics simulations.—All-atom MD simulations were performed using the CHARMM36(m) force fields for protein and lipids (Brooks et al., 2009; Klauda et al., 2010), with the TIP3P water model (Jorgensen et al., 1983) in 100 mM NaCl. All systems were prepared and equilibrated using CHARMM-GUI *Solution Builder* and *Membrane Builder* (Jo et al., 2008; Jo et al., 2009; Lee et al., 2019). The temperature and pressure were maintained at 318.15 K and 1 bar. MD production simulations were conducted with OpenMM (Eastman et al., 2013) for 1 μ s, and the last 500 ns of trajectories were used for analysis. The initial structural model was taken from the crystal structure of PHA7g; all ligands were removed and residues 236-254 were modeled using GalaxyFill, latest version (Ko et al., 2011).

Ten MD simulations were performed for each of the three membrane systems (Table S2), for a total of thirty independent simulations. The initial system size of each replica was 90 Å x 90 Å x 175 Å to accommodate for all initial components, yielding a total of approximately 125,000 atoms per replica. All analyses were performed using CHARMM, and models were visualized with VMD, version 1.9.4 (Humphrey et al., 1996) and PyMOL 2.2 (DeLano, 2002).

QUANTIFICATION AND STATISTICAL ANALYSIS

The ITC values in Table 1 represent the average of triplicate experiments performed for each ligand.

Supplementary Material

Refer to Web version on PubMed Central for supplementary material.

Acknowledgments

This work was supported by grants from the National Institutes of Health (GM118186, CA179087, CA160398, CA030199) and the National Science Foundation (MCB1810695).

Abbreviations:

4

IP(4,5)P₂	inositol (1,4,5) triphosphate
IP(3,4)P₂	inositol (1,3,4) triphosphate
IP(3,4,5)P₃	inositol (1,3,4,5) tetraphosphate
ITC	isothermal titration calorimetry
KRAS	Kirsten rat sarcoma viral oncogene homolog

MD	molecular dynamics
NMR	nuclear magnetic resonance
PH	pleckstrin homology
PIP	phosphatidyl inositol phosphate
PI(4,5)P₂	phosphatidyl inositol (4,5) diphosphate
PI(3,4)P₂	phosphatidyl inositol (3,4) diphosphate
PI(3,4,5)P₃	phosphatidyl inositol (3,4,5) triphosphate
PLEKHA7	pleckstrin homology domain containing family A member 7
HSQC	heteronuclear single quantum coherence

References

- Adams PD, Afonine PV, Bunkoczi G, Chen VB, Davis IW, Echols N, Headd JJ, Hung LW, Kapral GJ, Grosse-Kunstleve RW, et al. (2010). PHENIX: a comprehensive Python-based system for macromolecular structure solution. *Acta Crystallogr. D. Biol. Crystallogr.* 66, 213–221. [PubMed: 20124702]
- Awadalla MS, Thapa SS, Hewitt AW, Burdon KP, and Craig JE (2013). Association of genetic variants with primary angle closure glaucoma in two different populations. *PLoS One* 8, e67903. [PubMed: 23840785]
- Baker NA, Sept D, Joseph S, Holst MJ, and McCammon JA (2001). Electrostatics of nanosystems: application to microtubules and the ribosome. *Proc. Natl. Acad. Sci. U. S. A* 98, 10037–10041. [PubMed: 11517324]
- Bax A, and Grzesiek S (1993). Methodological advances in protein NMR. *Acc. Chem. Res* 26, 131–138.
- Bayburt TH, Grinkova YV, and Sligar SG (2002). Self-Assembly of Discoidal Phospholipid Bilayer Nanoparticles with Membrane Scaffold Proteins. *Nano Lett.* 2, 853–856.
- Brooks BR, Brooks CL 3rd, Mackerell AD Jr., Nilsson L, Petrella RJ, Roux B, Won Y, Archontis G, Bartels C, Boresch S, et al. (2009). CHARMM: the biomolecular simulation program. *J. Comput. Chem* 30, 1545–1614. [PubMed: 19444816]
- Cantley LC (2002). The phosphoinositide 3-kinase pathway. *Science* 296, 1655–1657. [PubMed: 12040186]
- Cao S, Chung S, Kim S, Li Z, Manor D, and Buck M (2019). K-Ras G-domain binding with signaling lipid phosphatidylinositol (4,5)-phosphate (PIP₂): membrane association, protein orientation, and function. *J. Biol. Chem* 294, 7068–7084. [PubMed: 30792310]
- Carpén JD, Faber AL, Horn C, Donoho GP, Briggs SL, Robbins CM, Hostetter G, Boguslawski S, Moses TY, Savage S, et al. (2007). A transforming mutation in the pleckstrin homology domain of AKT1 in cancer. *Nature* 448, 439–444. [PubMed: 17611497]
- Castellana B, Escuin D, Perez-Olabarria M, Vazquez T, Munoz J, Peiro G, Barnadas A, and Lerma E (2012). Genetic up-regulation and overexpression of PLEKHA7 differentiates invasive lobular carcinomas from invasive ductal carcinomas. *Hum. Pathol* 43, 1902–1909. [PubMed: 22542108]
- Cavanagh J, Fairbrother WJ, Palmer AG, and Skelton NJ (1996). *Protein NMR spectroscopy: principles and practice* (San Diego: Academic Press).
- Ceccarelli DF, Blasutig IM, Goudreaux M, Li Z, Ruston J, Pawson T, and Sicheri F (2007). Non-canonical interaction of phosphoinositides with pleckstrin homology domains of Tiam1 and ArhGAP9. *J. Biol. Chem* 282, 13864–13874. [PubMed: 17339315]

- Chen VB, Arendall WB 3rd, Headd JJ, Keedy DA, Immormino RM, Kapral GJ, Murray LW, Richardson JS, and Richardson DC (2010). MolProbity: all-atom structure validation for macromolecular crystallography. *Acta Crystallogr. D. Biol. Crystallogr* 66, 12–21. [PubMed: 20057044]
- Clore GM, and Gronenborn AM (1998). NMR structure determination of proteins and protein complexes larger than 20 kDa. *Curr. Opin. Chem. Biol* 2, 564–570. [PubMed: 9818180]
- Cornilescu G, Delaglio F, and Bax A (1999). Protein backbone angle restraints from searching a database for chemical shift and sequence homology. *J. Biomol. NMR* 13, 289–302. [PubMed: 10212987]
- Cowan SW, Newcomer ME, and Jones TA (1990). Crystallographic refinement of human serum retinol binding protein at 2A resolution. *Proteins* 8, 44–61. [PubMed: 2217163]
- Cronin TC, DiNitto JP, Czech MP, and Lambright DG (2004). Structural determinants of phosphoinositide selectivity in splice variants of Grp1 family PH domains. *EMBO J.* 23, 3711–3720. [PubMed: 15359279]
- Delaglio F, Grzesiek S, Vuister GW, Zhu G, Pfeifer J, and Bax A (1995). NMRPipe: a multidimensional spectral processing system based on UNIX pipes. *J. Biomol. NMR* 6, 277–293. [PubMed: 8520220]
- DeLano WL (2002). PyMOL: An Open-Source Molecular Graphics Tool. *CCP4 Newsletter On Protein Crystallography* 1, 82–92.
- Ding Y, Fujimoto LM, Yao Y, Plano GV, and Marassi FM (2015). Influence of the lipid membrane environment on structure and activity of the outer membrane protein Ail from *Yersinia pestis*. *Biochim Biophys Acta* 1848, 712–720. [PubMed: 25433311]
- DiNitto JP, and Lambright DG (2006). Membrane and juxtamembrane targeting by PH and PTB domains. *Biochim Biophys Acta* 1761, 850–867. [PubMed: 16807090]
- Eastman P, Friedrichs MS, Chodera JD, Radmer RJ, Bruns CM, Ku JP, Beauchamp KA, Lane TJ, Wang LP, Shukla D, et al. (2013). OpenMM 4: A Reusable, Extensible, Hardware Independent Library for High Performance Molecular Simulation. *Journal of chemical theory and computation* 9, 461–469. [PubMed: 23316124]
- Emsley P, Lohkamp B, Scott WG, and Cowtan K (2010). Features and development of Coot. *Acta Crystallogr. D. Biol. Crystallogr* 66, 486–501. [PubMed: 20383002]
- Ferentz AE, and Wagner G (2000). NMR spectroscopy: a multifaceted approach to macromolecular structure. *Q. Rev. Biophys* 33, 29–65. [PubMed: 11075388]
- Ferguson KM, Kavran JM, Sankaran VG, Fournier E, Isakoff SJ, Skolnik EY, and Lemmon MA (2000). Structural basis for discrimination of 3-phosphoinositides by pleckstrin homology domains. *Mol. Cell* 6, 373–384. [PubMed: 10983984]
- Fesik SW, and Zuurweg ER (1990). Heteronuclear three-dimensional NMR spectroscopy of isotopically labelled biological macromolecules. *Q. Rev. Biophys* 23, 97–131. [PubMed: 2188281]
- Goddard TD, and Kneller DG (2004). SPARKY 3, University of California, San Francisco.
- Grzesiek S, and Bax A (1992). Improved 3D triple-resonance NMR techniques applied to a 31 kDa protein. *J. Magn. Reson* 96, 432–440.
- Hahn F, Eitzkorn M, Raschle T, and Wagner G (2013). Optimized phospholipid bilayer nanodiscs facilitate high-resolution structure determination of membrane proteins. *J. Am. Chem. Soc* 135, 1919–1925. [PubMed: 23294159]
- Humphrey W, Dalke A, and Schulten K (1996). VMD: visual molecular dynamics. *J. Mol. Graph* 14, 33–38, 27–38. [PubMed: 8744570]
- Hyvonen M, Macias MJ, Nilges M, Oschkinat H, Saraste M, and Wilmanns M (1995). Structure of the binding site for inositol phosphates in a PH domain. *EMBO J.* 14, 4676–4685. [PubMed: 7588597]
- Indarte M, Puentes R, Maruggi M, Ihle NT, Grandjean G, Scott M, Ahmed Z, Meuillet EJ, Zang S, Lemos R Jr., et al. (2019). An Inhibitor of the Pleckstrin Homology Domain of CNK1 Selectively Blocks the Growth of Mutant KRAS Cells and Tumors. *Cancer Res.* 79, 3100–3111. [PubMed: 31040156]
- Jencks WP (1981). On the attribution and additivity of binding energies. *Proc. Natl. Acad. Sci. U. S. A* 78, 4046–4050. [PubMed: 16593049]

- Jeung H-C, Kiriakova G, Kirkpatrick L, Indarte M, and Powis G (2011). Abstract A199: The pleckstrin-homology-domain-containing protein PLEKHA7 is a novel target for selectively inhibiting mutant KRAS colon cancer cell proliferation. *Mol. Cancer Ther* 10, A199.
- Jian X, Tang WK, Zhai P, Roy NS, Luo R, Gruschus JM, Yohe ME, Chen PW, Li Y, Byrd RA, et al. (2015). Molecular Basis for Cooperative Binding of Anionic Phospholipids to the PH Domain of the Arf GAP ASAP1. *Structure* 23, 1977–1988. [PubMed: 26365802]
- Jo S, Kim T, Iyer VG, and Im W (2008). CHARMM-GUI: a web-based graphical user interface for CHARMM. *J. Comput. Chem* 29, 1859–1865. [PubMed: 18351591]
- Jo S, Lim JB, Klauda JB, and Im W (2009). CHARMM-GUI Membrane Builder for mixed bilayers and its application to yeast membranes. *Biophys. J* 97, 50–58. [PubMed: 19580743]
- Johnson BA, and Blevins RA (1994). NMR View: A computer program for the visualization and analysis of NMR data. *J. Biomol. NMR* 4, 603–614. [PubMed: 22911360]
- Jorgensen WL, Chandrasekhar J, Madura JD, Impey RW, and Klein ML (1983). Comparison of simple potential functions for simulating liquid water. *The Journal of Chemical Physics* 79, 926–935.
- Kay LE (2001). Nuclear magnetic resonance methods for high molecular weight proteins: a study involving a complex of maltose binding protein and beta-cyclodextrin. *Methods Enzymol.* 339, 174–203. [PubMed: 11462811]
- Klauda JB, Venable RM, Freites JA, O'Connor JW, Tobias DJ, Mondragon-Ramirez C, Vorobyov I, MacKerell AD Jr., and Pastor RW (2010). Update of the CHARMM all-atom additive force field for lipids: validation on six lipid types. *J Phys Chem B* 114, 7830–7843. [PubMed: 20496934]
- Ko J, Lee D, Park H, Coutsiaris EA, Lee J, and Seok C (2011). The FALC-Loop web server for protein loop modeling. *Nucleic Acids Res* 39, W210–214. [PubMed: 21576220]
- Kourtidis A, Ngok SP, Pulimeno P, Feathers RW, Carpio LR, Baker TR, Carr JM, Yan IK, Borges S, Perez EA, et al. (2015). Distinct E-cadherin-based complexes regulate cell behaviour through miRNA processing or Src and p120 catenin activity. *Nat Cell Biol* 17, 1145–1157. [PubMed: 26302406]
- Lai CL, Srivastava A, Pilling C, Chase AR, Falke JJ, and Voth GA (2013). Molecular mechanism of membrane binding of the GRP1 PH domain. *J. Mol. Biol* 425, 3073–3090. [PubMed: 23747485]
- Lee J, Patel DS, Stahle J, Park SJ, Kern NR, Kim S, Lee J, Cheng X, Valvano MA, Holst O, et al. (2019). CHARMM-GUI Membrane Builder for Complex Biological Membrane Simulations with Glycolipids and Lipoglycans. *Journal of chemical theory and computation* 15, 775–786. [PubMed: 30525595]
- Lemmon MA (2007). Pleckstrin homology (PH) domains and phosphoinositides. *Biochem. Soc. Symp*, 81–93. [PubMed: 17233582]
- Lenoir M, Coskun U, Grzybek M, Cao X, Buschhorn SB, James J, Simons K, and Overduin M (2010). Structural basis of wedging the Golgi membrane by FAPP pleckstrin homology domains. *EMBO Rep* 11, 279–284. [PubMed: 20300118]
- Levy D, Ehret GB, Rice K, Verwoert GC, Launer LJ, Dehghan A, Glazer NL, Morrison AC, Johnson AD, Aspelund T, et al. (2009). Genome-wide association study of blood pressure and hypertension. *Nat. Genet* 41, 677–687. [PubMed: 19430479]
- Lietzke SE, Bose S, Cronin T, Klarlund J, Chawla A, Czech MP, and Lambright DG (2000). Structural basis of 3-phosphoinositide recognition by pleckstrin homology domains. *Mol. Cell* 6, 385–394. [PubMed: 10983985]
- Lumb CN, He J, Xue Y, Stansfeld PJ, Stahelin RV, Kutateladze TG, and Sansom MS (2011). Biophysical and computational studies of membrane penetration by the GRP1 pleckstrin homology domain. *Structure* 19, 1338–1346. [PubMed: 21893292]
- Macias MJ, Musacchio A, Ponstingl H, Nilges M, Saraste M, and Oschkinat H (1994). Structure of the pleckstrin homology domain from beta-spectrin. *Nature* 369, 675–677. [PubMed: 8208297]
- McCoy AJ, Grosse-Kunstleve RW, Adams PD, Winn MD, Storoni LC, and Read RJ (2007). Phaser crystallographic software. *J. Appl. Crystallogr* 40, 658–674. [PubMed: 19461840]
- Meng W, Mushika Y, Ichii T, and Takeichi M (2008). Anchorage of microtubule minus ends to adherens junctions regulates epithelial cell-cell contacts. *Cell* 135, 948–959. [PubMed: 19041755]
- Meuillet EJ, Mahadevan D, Vankayalapati H, Berggren M, Williams R, Coon A, Kozikowski AP, and Powis G (2003). Specific inhibition of the Akt1 pleckstrin homology domain by D-3-

- deoxy-phosphatidyl-myo-inositol analogues. *Molecular cancer therapeutics* 2, 389–399. [PubMed: 12700283]
- Meuillet EJ, Zuohe S, Lemos R, Ihle N, Kingston J, Watkins R, Moses SA, Zhang S, Du-Cuny L, Herbst R, et al. (2010). Molecular pharmacology and antitumor activity of PHT-427, a novel Akt/phosphatidylinositide-dependent protein kinase 1 pleckstrin homology domain inhibitor. *Molecular cancer therapeutics* 9, 706–717. [PubMed: 20197390]
- Moravcevic K, Oxley CL, and Lemmon MA (2012). Conditional peripheral membrane proteins: facing up to limited specificity. *Structure* 20, 15–27. [PubMed: 22193136]
- Murshudov GN, Skubák P, Lebedev AA, Pannu NS, Steiner RA, Nicholls RA, Winn MD, Long F, and Vagin AA (2011). REFMAC5 for the refinement of macromolecular crystal structures. *Acta crystallographica. Section D, Biological crystallography* 67, 355–367. [PubMed: 21460454]
- Nair-Menon J, Daulagala AC, Connor DM, Rutledge L, Penix T, Bridges MC, Wellslager B, Spyropoulos DD, Timmers CD, Broome AM, et al. (2020). Predominant Distribution of the RNAi Machinery at Apical Adherens Junctions in Colonic Epithelia Is Disrupted in Cancer. *Int J Mol Sci* 21.
- Ni T, Kalli AC, Naughton FB, Yates LA, Naneh O, Kozorog M, Anderluh G, Sansom MS, and Gilbert RJ (2017). Structure and lipid-binding properties of the kindlin-3 pleckstrin homology domain. *Biochem. J* 474, 539–556. [PubMed: 27974389]
- Paschoud S, Jond L, Guerrero D, and Citi S (2014). PLEKHA7 modulates epithelial tight junction barrier function. *Tissue Barriers* 2, e28755. [PubMed: 24843844]
- Pulimeno P, Bauer C, Stutz J, and Citi S (2010). PLEKHA7 is an adherens junction protein with a tissue distribution and subcellular localization distinct from ZO-1 and E-cadherin. *PLoS One* 5, e12207. [PubMed: 20808826]
- Rouaud F, Sluysmans S, Flinois A, Shah J, Vasileva E, and Citi S (2020). Scaffolding proteins of vertebrate apical junctions: structure, functions and biophysics. *Biochim Biophys Acta Biomembr* 1862, 183399. [PubMed: 32553946]
- Sacchettini JC, Gordon JI, and Banaszak LJ (1989). Crystal structure of rat intestinal fatty-acid-binding protein. Refinement and analysis of the Escherichia coli-derived protein with bound palmitate. *J Mol Biol* 208, 327–339. [PubMed: 2671390]
- Shen Y, Delaglio F, Cornilescu G, and Bax A (2009). TALOS+: a hybrid method for predicting protein backbone torsion angles from NMR chemical shifts. *J. Biomol. NMR* 44, 213–223. [PubMed: 19548092]
- Soubias O, Pant S, Heinrich F, Zhang Y, Roy NS, Li J, Jian X, Yohe ME, Randazzo PA, Losche M, et al. (2020). Membrane surface recognition by the ASAP1 PH domain and consequences for interactions with the small GTPase Arf1. *Sci Adv* 6.
- Thomas CC, Dowler S, Deak M, Alessi DR, and van Aalten DM (2001). Crystal structure of the phosphatidylinositol 3,4-bisphosphate-binding pleckstrin homology (PH) domain of tandem PH-domain-containing protein 1 (TAPP1): molecular basis of lipid specificity. *Biochem. J* 358, 287–294. [PubMed: 11513726]
- Tille JC, Ho L, Shah J, Seyde O, McKee TA, and Citi S (2015). The Expression of the Zonula Adhaerens Protein PLEKHA7 Is Strongly Decreased in High Grade Ductal and Lobular Breast Carcinomas. *PLoS One* 10, e0135442. [PubMed: 26270346]
- Wen Y, Vogt VM, and Feigenson GW (2018). Multivalent Cation-Bridged PI(4,5)P2 Clusters Form at Very Low Concentrations. *Biophys. J* 114, 2630–2639. [PubMed: 29874613]
- Williamson MP (2013). Using chemical shift perturbation to characterise ligand binding. *Prog. Nucl. Magn. Reson. Spectrosc* 73, 1–16. [PubMed: 23962882]
- Winn MD, Ballard CC, Cowtan KD, Dodson EJ, Emsley P, Evans PR, Keegan RM, Krissinel EB, Leslie AG, McCoy A, et al. (2011). Overview of the CCP4 suite and current developments. *Acta Crystallogr. D. Biol. Crystallogr* 67, 235–242. [PubMed: 21460441]
- Wittekind M, and Mueller L (1993). HNCACB, a High-Sensitivity 3D NMR Experiment to Correlate Amide-Proton and Nitrogen Resonances with the Alpha- and Beta-Carbon Resonances in Proteins. *J. Magn. Reson. B* 101, 201–205.

- Wythe JD, Jurynech MJ, Urness LD, Jones CA, Sabeh MK, Werdich AA, Sato M, Yost HJ, Grunwald DJ, Macrae CA, et al. (2011). Hadp1, a newly identified pleckstrin homology domain protein, is required for cardiac contractility in zebrafish. *Dis Model Mech* 4, 607–621. [PubMed: 21628396]
- Yamamoto E, Domanski J, Naughton FB, Best RB, Kalli AC, Stansfeld PJ, and Sansom MSP (2020). Multiple lipid binding sites determine the affinity of PH domains for phosphoinositide-containing membranes. *Sci Adv* 6, eaay5736. [PubMed: 32128410]
- Yoon HS, Hajduk PJ, Petros AM, Olejniczak ET, Meadows RP, and Fesik SW (1994). Solution structure of a pleckstrin homology domain. *Nature* 369, 672–675. [PubMed: 8208296]

Highlights

- The structure of the PLEHA7 PH domain reveals multiple binding sites for PIP lipids.
- The PH domain contains major elements of PIP recognition by PLEKHA7.
- The membrane scaffold promotes multivalent association of one PH domain with PIPs.
- The PLEKHA7 PH domain induces membrane PIP clustering.

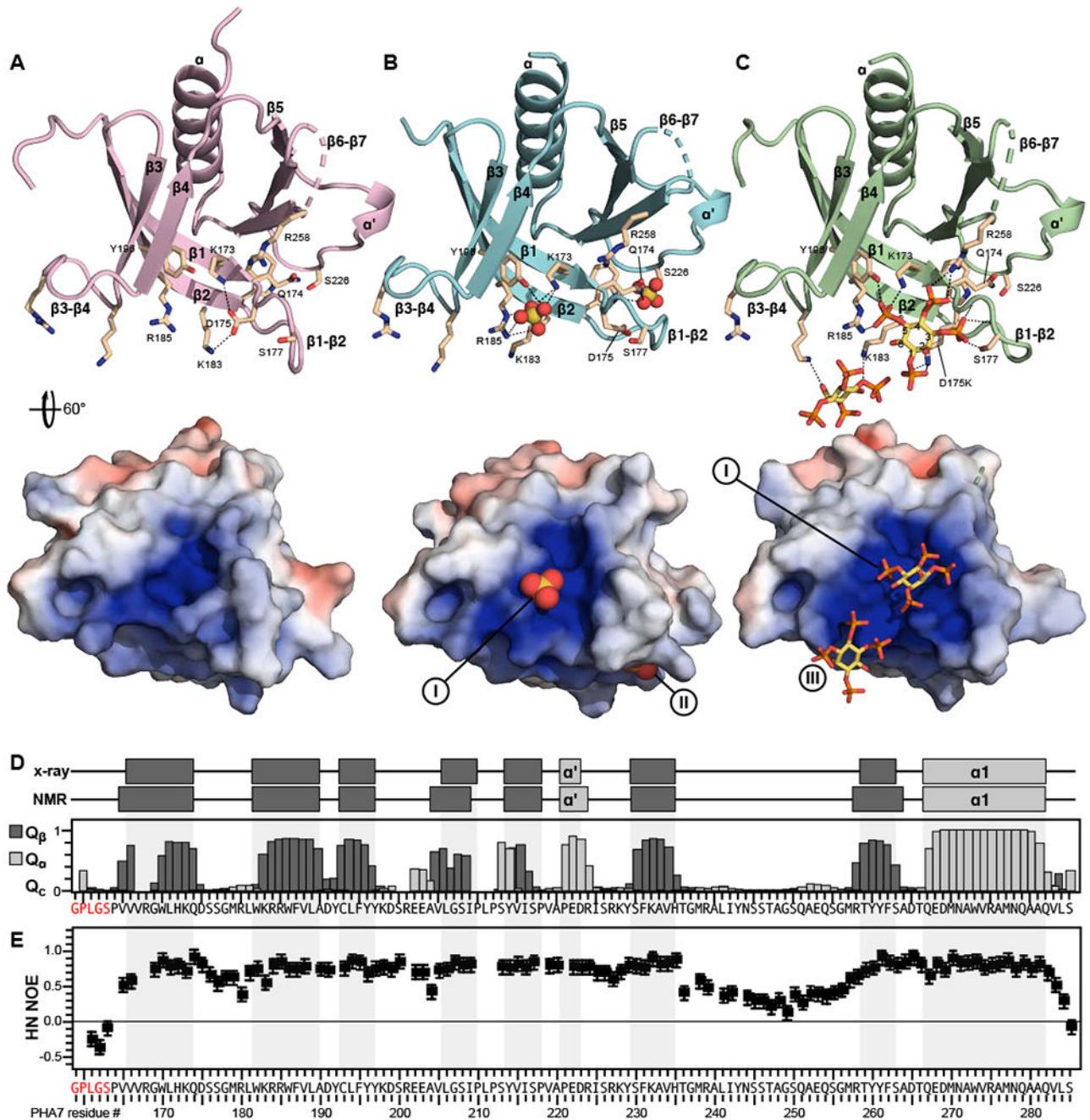


Fig. 1. Structure of the PLEKHA7 PHD.

(A) PHA7_{APO}. (B) PHA7_S bound to sulfate (yellow/orange spheres). (C) Mutant PHA7-D175K bound to soluble IP(3,4,5)P₃ (yellow/orange sticks). Key residues are shown as sticks. Dashes denote protein-protein, protein-sulfate or protein-IP(3,4,5)P₃ polar contacts (<4Å). The 60° surface representations are colored by electrostatic potential from -5 kT/e (red) to +5 kT/e (blue). The positions of the three binding sites (I-III) for sulfate or phosphate are marked. (D, E) Structure and dynamics of PHA7 (164-285) derived from NMR. (D) The secondary structure was derived from TALOS chemical shift analysis. Bars

depict the accuracy (Q) of prediction for α -helix (Q- α), β -strand (Q- β), or random coil (Q-c). Elements of the secondary structure derived from crystallography and NMR are depicted above the plot. (B) The heteronuclear $^1\text{H}/^{15}\text{N}$ NOE relative intensities reflect dynamics of PHA7_{APO}.

Author Manuscript

Author Manuscript

Author Manuscript

Author Manuscript

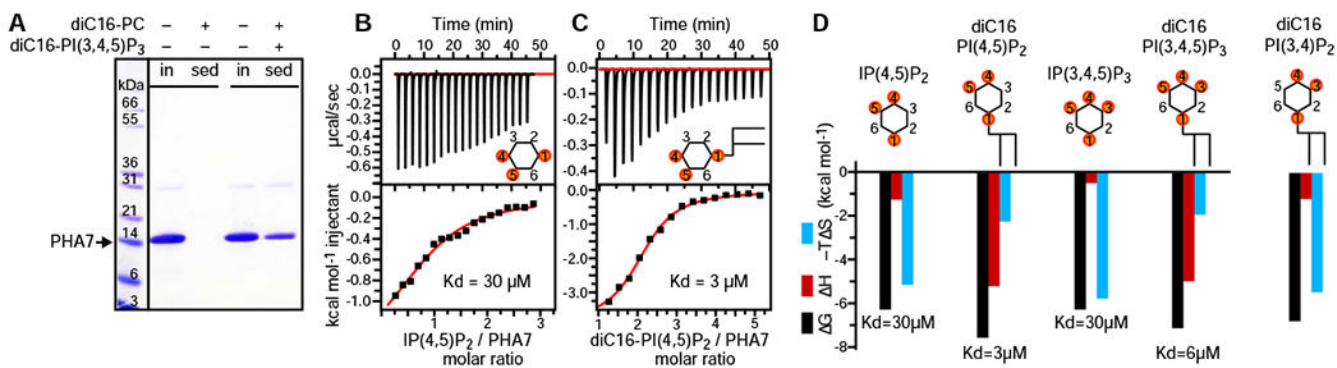


Fig. 2. Interactions of PHA7 with PIP lipids and soluble IPs.

(A) SDS-PAGE analysis of PHA7 co-sedimentation with diC16-PC liposomes prepared with or without 10% molar diC16-PI(3,4,5)P₃. Monomeric PHA7 (arrow) migrates with apparent molecular weight of ~15 kDa. (B-D) Representative ITC binding isotherms (B, C) and free energies (D) measured for titrations of PHA7 with soluble IP(4,5)P₂ and IP(3,4,5)P₃, or nanodiscs containing 10% molar diC16-PI(4,5)P₂ and diC16-PI(3,4,5)P₃. Continuous red lines are the best fits of the data to a single-site binding model, used to extract the values of the dissociation constant (K_d).

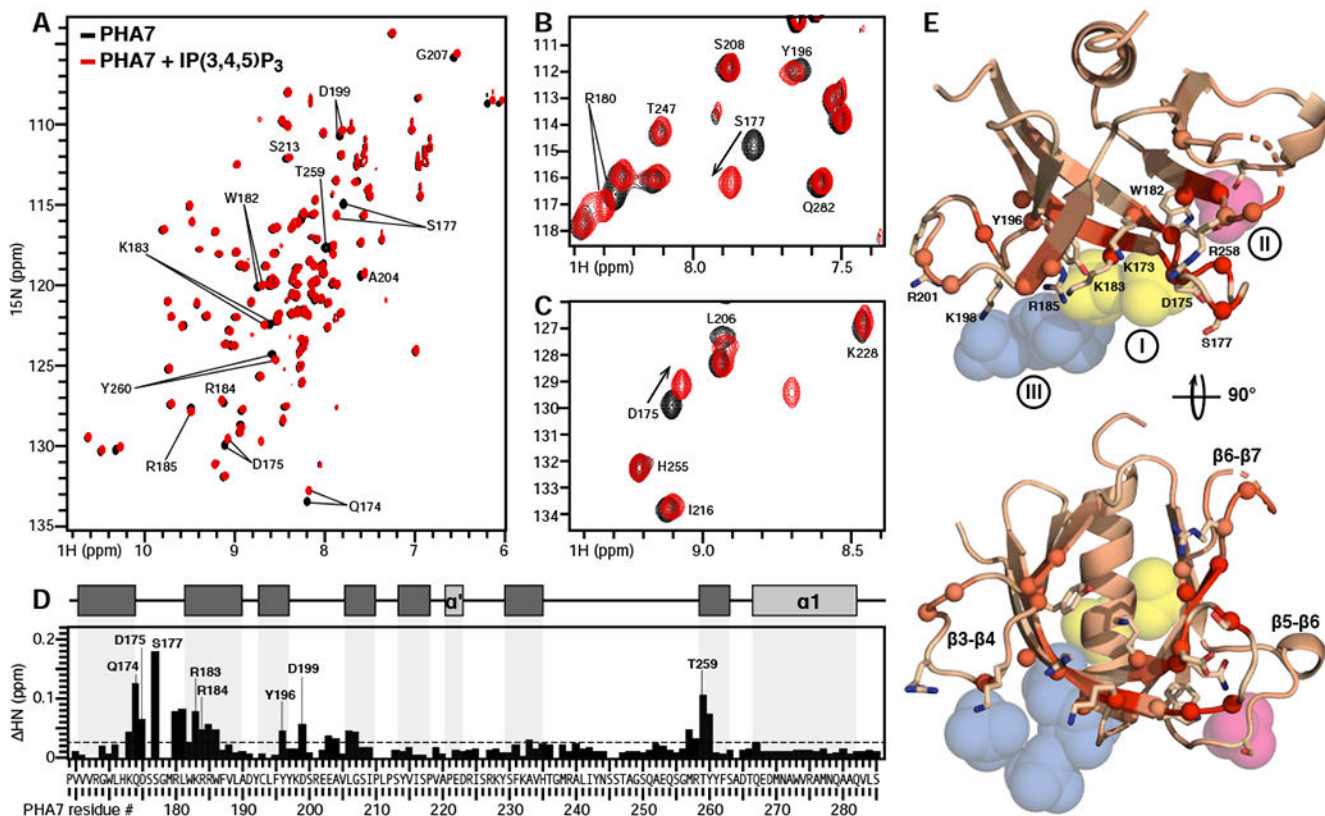


Fig. 3. Interaction map of PHA7 with soluble IP(3,4,5) P_3 .

(A-C) $^1\text{H}/^{15}\text{N}$ HSQC NMR spectra of ^{15}N labeled wild-type PHA7 domain acquired with (red) or without (black) 1.5 molar equivalents of soluble IP(3,4,5) P_3 . The spectra were acquired at 15°C . Selected regions of the spectra are expanded (B) to highlight specific perturbation sites. (D) Profile of $^1\text{H}/^{15}\text{N}$ chemical shift perturbations induced by IP(3,4,5) P_3 across the sequence of PHA7. Bars represent the combined difference (ΔHN) of amide ^1H and ^{15}N chemical shifts. The protein secondary structure is outlined at the top. (E) Orthogonal views of the structure of PHA7 $_{\Delta\text{PO}}$. Colors reflect the magnitude of ΔHN from 0 ppm (wheat) to the maximum value (red). Highly perturbed sites (> 1 standard deviation of the values of ΔHN) have CA atoms shown as spheres. Key side chains of three IP binding sites (I-III) are shown as sticks. The positions of sulfate or phosphate groups identified in the structures of PHA7 $_{\text{s}}$ and PHA7-D175K are shown as spheres, superimposed on the structural model. They denote binding sites I (yellow), II (pink) and III (blue).

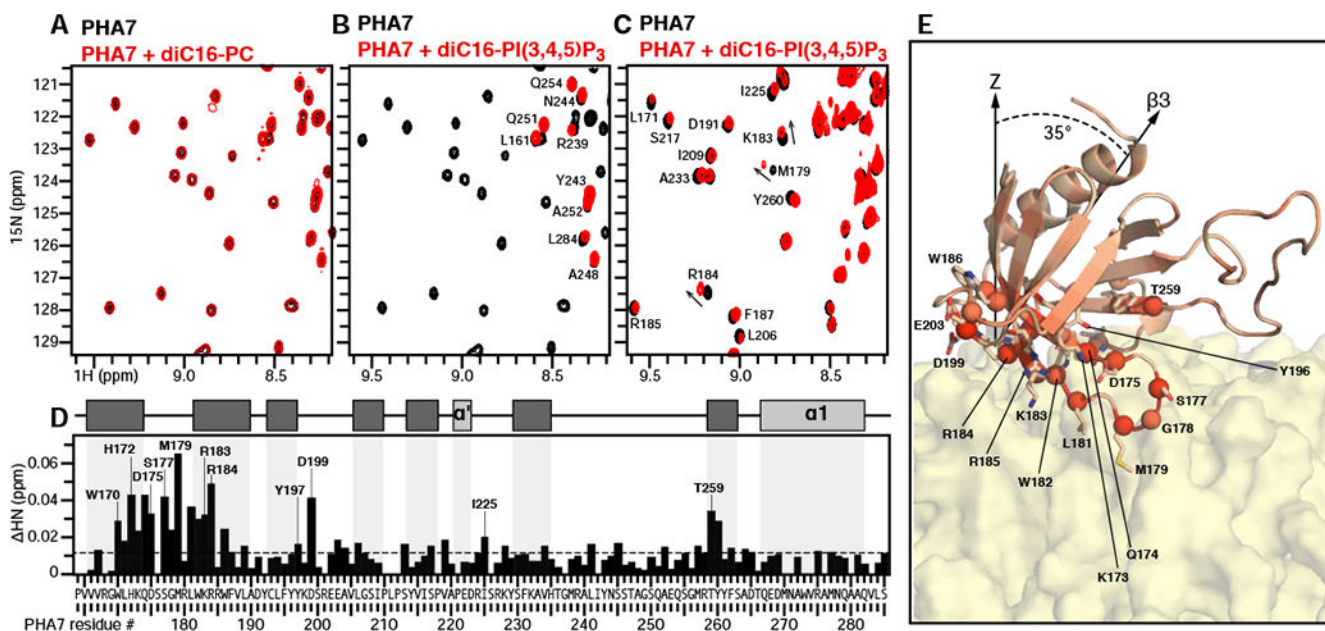


Fig. 4. Interaction map of PLEKHA7 with diC16-PI(3,4,5)P₃ nanodiscs.

(A–C) ¹H/¹⁵N HSQC NMR spectra of ¹⁵N-labeled wild-type PHA7 obtained before (black) or after (red) incubation with 1.5 molar equivalents of lipid nanodiscs prepared with 100% diC16-PC (A), or 9/1 molar diC16-PC and diC16-PI(3,4,5)P₃ (B, C). The spectra were acquired at 15°C (A, B) or 45°C (C). Peaks that do not change in the presence of diC16-PIP nanodiscs are labeled (B). (D) Profile of ¹H/¹⁵N chemical shift perturbations induced by the association of PHA7 with diC16-PI(3,4,5)P₃ nanodiscs, at 45°C, across the protein sequence. (E) Snapshot (taken at 890 ns) of a MD simulation of PHA7 with a diC16-PI(3,4,5)P₃-rich lipid bilayer membrane. PHA7 colors reflect the magnitude of NMR chemical shift perturbation from 0 ppm (wheat) to the maximum value (red). Highly perturbed sites (> 1 standard deviation of the values of ¹HN) have CA atoms shown as spheres and side chains shown as sticks. The membrane is represented as a molecular surface.

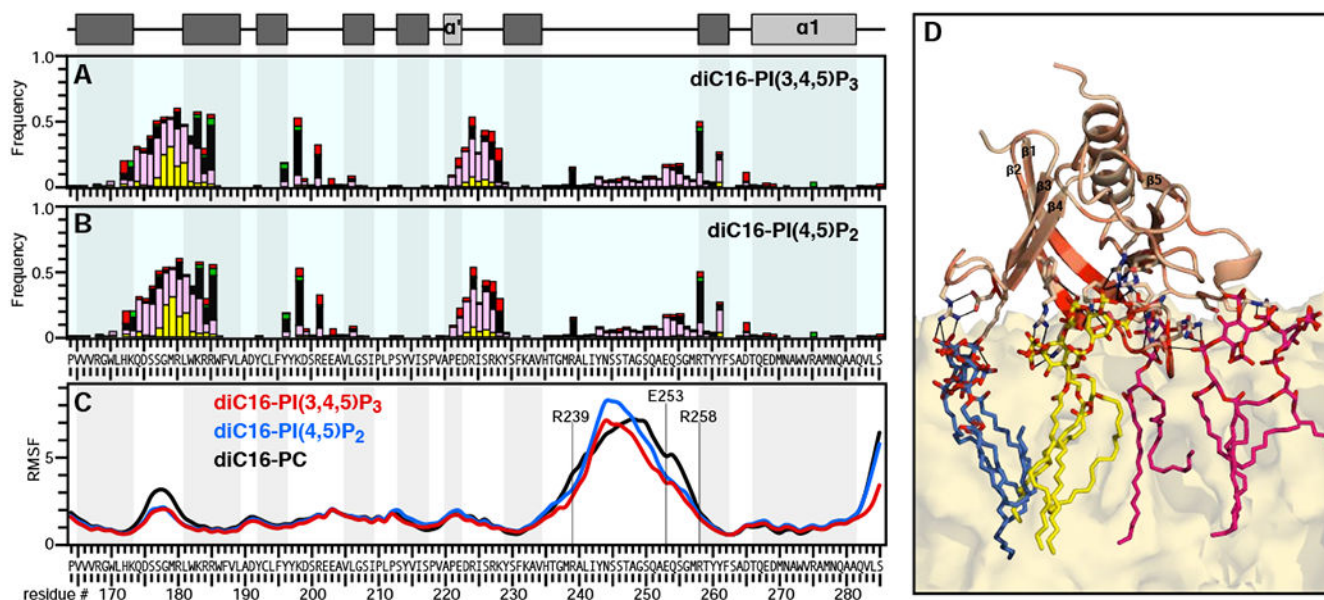


Fig. 5. Structure and dynamics of the PLEKHA7 PH domain.

(A, B) MD interaction profile of PHA7 with diC16-PI(3,4,5)P₃ or diC16-PI(4,5)P₂ membranes. The bars represent frequency of occurrence within 4 Å of water (light blue), Na⁺ (red) or Cl⁻ (green) ions, phospholipid tails (yellow), PC headgroups (pink), or PIP headgroups (black). Each data point is the average of ten independent MD simulations over the last 500 ns of 1- μ s MD trajectories. (C) MD time-averaged RMSF calculated for PHA7 heavy atoms over the last 500 ns of 1- μ s MD trajectories for ten independent simulations in diC16-PI(3,4,5)P₃ (red), diC16-PI(4,5)P₂ (blue), or diC16-PC (black) membranes. (D) Snapshot (taken at 890 ns) of MD simulation of PHA7 with a diC16-PI(3,4,5)P₃ membrane. PHA7 colors reflect the magnitude of NMR chemical shift perturbation from 0 ppm (wheat) to the maximum value (red). Key side chains with close (< 4 Å) contacts to PIP headgroups are shown as sticks. The membrane is represented as a molecular surface (yellow). Colors of bound PIP molecules (lines) represent their association with binding sites I (yellow), II (pink), or III (blue).

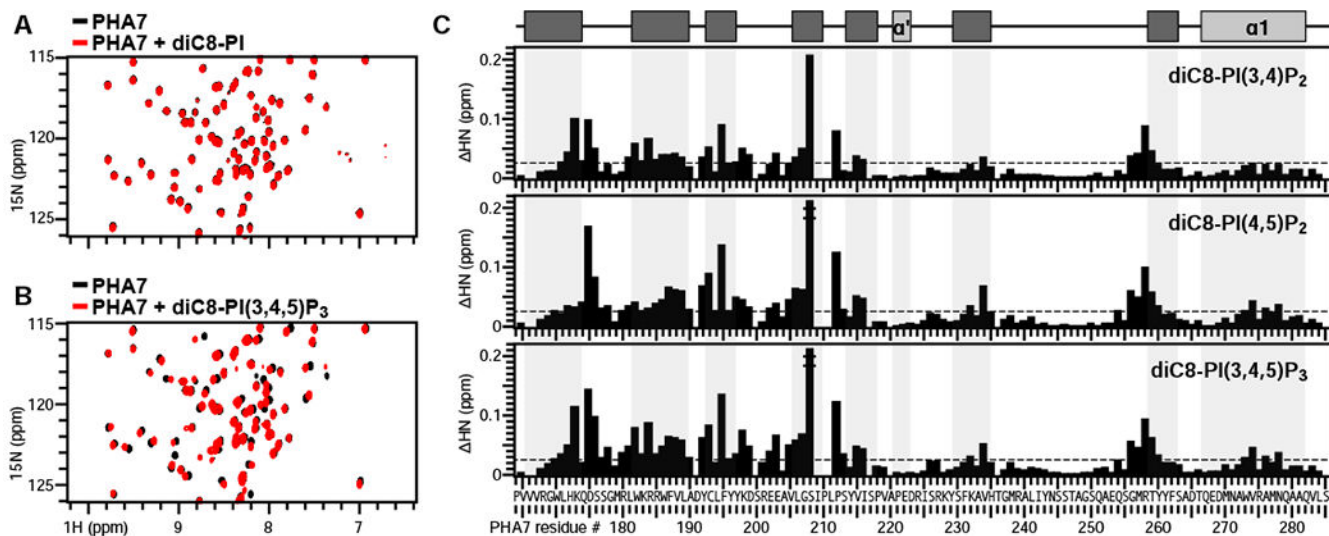


Fig. 6. Interaction map of PHA7 with soluble short-chain diC8-PIPs.

(A,B) Selected regions of the $^1\text{H}/^{15}\text{N}$ HSQC NMR spectra of ^{15}N labeled wild-type PHA7 domain acquired with (red) or without (black) 1.5 molar equivalents of short-chain diC8-PI(3,4,5)P₃ or diC8-PI, at 15°C. (C) Profiles of $^1\text{H}/^{15}\text{N}$ chemical shift perturbations induced by diC8-PIPs across the sequence of PHA7. Bars represent the combined difference (ΔHN) of amide ^1H and ^{15}N chemical shifts. The protein secondary structure is outlined at the top.

Table 1.

ITC values of K_d (μM) for the interactions of wild-type PHA7 or mutant PHA7-D175K with soluble IP headgroups or diC16-phosphatidyl inositol (diC 16-PI) incorporated in lipid nanodiscs. Each value represents the average of triplicate experiments.

	IP(4,5)P ₂ or PI(4,5)P ₂		IP(3,4,5)P ₃ or PI(3,4,5)P ₃		IP(3,4)P ₂ or PI(3,4)P ₂
	PHA7	PHA7-D175K	PHA7	PHA7-D175K	PHA7
soluble IP	30.5 ± 0.6	10.7 ± 0.2	30.1 ± 2.3	3.5 ± 0.5	–
nanodisc diC16-PI	3.0 ± 1.2	0.5 ± 0.1	6.2 ± 0.2	5.5 ± 0.1	9.0 ± 0.3

Author Manuscript

Author Manuscript

Author Manuscript

Author Manuscript

KEY RESOURCES TABLE

REAGENT or RESOURCE	SOURCE	IDENTIFIER
Bacterial and virus strains		
<i>E. coli</i> BL21(DE3) cells	Invitrogen	Cat: C600003
Recombinant DNA		
pGEX-6P-1 Plasmid Vector	Sigma	Cat: GE28-9546-48
Chemicals, peptides, and recombinant proteins		
(¹⁵ NH ₄) ₂ SO ₄	Cambridge Isotope Laboratories	NLM-713
¹³ C-glucose	Cambridge Isotope Laboratories	CLM-1396
diC16-PC	Avanti Polar Lipids	850355
diC16-PI(4,5)P ₂	Echelon	P-4516
diC16-PI(3,4)P ₂	Echelon	P-3416
diC16-PI(3,4,5)P ₃	Echelon	P-3916
Deposited data		
Structure of PLEKHA7 PH domain (PHA7 _{AP0})	This paper	PDB: 7kk7
crystal structure of PLEKHA7 PH domain binding SO ₄ (PHA7 _S)	This paper	PDB: 7kjo
crystal structure of PLEKHA7 PH domain binding inositol-tetraphosphate (PHA7-D175K)	This paper	PDB: 7kjz
NMR chemical shifts of PLEKHA7 PH domain	This paper	BMRB: 50512
Structure of PLEKHA1 PH domain (PHA1)	(Thomas et al., 2001)	PDB: 1eaz
Structure of PLEKHA3 PH domain (PHA3)	(Lenoir et al., 2010)	PDB: 2kcj
Structure of PLEKHA4 PH domain (PHA4)	Milburn, Komande, Deak, Alessi, Van Aalten (2003). To be published.	PDB: 1upq
Structure of PLEKHA5 PH domain (PHA5)	Li, Tomizawa, Koshiba, Inoue, Kigawa, Yokoyama (2006). To be published.	PDB: 2dkp
Structure of PLEKHA6 PH domain (PHA6)	Li, Tomizawa, Koshiba, Inoue, Kigawa, Yokoyama (2007). To be published.	PDB: 2yry
Structure of ANLN PH domain	Vollmar, Wang., Krojer, Elkins, Filippakopoulos, Ugochukwu, Cocking, von Delft, Bountra, Arrowsmith, Weigelt, Edwards, Knapp (2011). To be published.	PDB: 2y7b
Structure of GRP1 PH domain	(Lietzke et al., 2000)	PDB: 1fgy
Structure of ARNO PH domain	(Cronin et al., 2004)	PDB: 1u27
Structure of DAPP1 PH domain	(Ferguson et al., 2000)	PDB: 1fao
Software and algorithms		
NMRPipe	(Delaglio et al., 1995)	https://spin.niddk.nih.gov/bax/software/NMRPipe/NMRPipe.html
Sparky	(Goddard and Kneller, 2004)	https://www.cgl.ucsf.edu/home/sparky/
NMRView	(Johnson and Blevins, 1994)	http://www.onemoonscientific.com/

REAGENT or RESOURCE	SOURCE	IDENTIFIER
TopSpin	Bruker Biospin	https://www.bruker.com/products/mr/nmr/software/topspin.html
PyMol	Schroedinger (DeLano, 2002)	https://pymol.org/2/
PHENIX	(Adams et al., 2010)	http://www.phenix-online.org/
CCP4	(Winn et al., 2011)	http://www.ccp4.ac.uk/
COOT	(Emsley et al., 2010)	https://www2.mrc-lmb.cam.ac.uk/personal/pemsley/coot/
Molprobit	(Chen et al., 2010)	http://molprobit.biochem.duke.edu/
CHARMM36(m)	(Brooks et al., 2009; Klauda et al., 2010)	https://www.charmm.org/
CHARMM-GUI	(Jo et al., 2008; Jo et al., 2009; Lee et al., 2019)	http://www.charmm-gui.org/

Author Manuscript

Author Manuscript

Author Manuscript

Author Manuscript